Crystal structure, stoichiometry, and dielectric relaxation in $Bi_{3.32}Nb_{7.09}O_{22.7}$ and structurally related ternary phases

I.E. Grey[a,*], T.A. Vanderah[b], W.G. Mumme[a], R.S. Roth[b], J. Guzman[c], J.C. Nino[c], I. Levin[b]

[a]CSIRO Minerals, Box 312 Clayton South, Victoria 3169, Australia
[b]Materials Science and Engineering Laboratory, National Institute of Standards and Technology, Gaithersberg, MD 20899, USA
[c]Department of Materials Science and Engineering, University of Florida, Gainesville, FL 32611, USA

Abstract

The crystal structure of the phase previously reported to occur at 4:9 $Bi_2O_3:Nb_2O_5$ has been determined using single-crystal X-ray and powder neutron diffraction ($P6_3/mmc$; $a = 7.4363(1)$ Å, $c = 19.7587(5)$ Å; $Z = 2$). The structural study combined with phase equilibrium analyses indicate that the actual composition is $Bi_{3.32}Nb_{7.09}O_{22.7}$. This binary compound is the end-member of a family of four phases which form along a line between it and the pyrochlore phase field in the $Bi_2O_3:Fe_2O_3:Nb_2O_5$ system. The structures are derived from the parent pyrochlore end-member by chemical twinning, and can also be described as unit-cell intergrowths of the pyrochlore and hexagonal tungsten bronze (HTB) structures. The dielectric properties of the three chemically twinned pyrochlore phases, $Bi_{3.32}Nb_{7.09}O_{22.7}$, $Bi_{9.3}Fe_{1.1}Nb_{16.9}O_{57.8}$ and $Bi_{5.67}FeNb_{10}O_{35}$, were characterized. All exhibit low-temperature, broad dielectric relaxation similar to that of the Bi–Fe–Nb–O pyrochlore. At 1 MHz and ≈ 175 K the observed relative permittivites were 345, 240, and 205, respectively, compared to 125 for the Bi–Fe–Nb–O pyrochlore. The higher relative permittivities observed for the chemically twinned pyrochlore derivatives are ascribed to the presence of HTB blocks in their structures: The Bi atoms located in the HTB blocks feature highly asymmetric coordination environments compared to pyrochlore, and the magnitude of the relative permittivity increases with the proportion of Bi located within the HTB portions of the structures.
© 2008 Elsevier Inc. All rights reserved.

Keywords: Crystal structure of new bismuth niobate; Dielectric relaxation in bismuth niobates; Chemically twinned pyrochlore phases; Structure of $Bi_{3.32}Nb_{7.09}O_{22.7}$

1. Introduction

We have recently reported [1] the structural characterisation of two new ternary bismuth iron niobates with structures based on chemical twinning of pyrochlore (py). $Bi_{5.67}FeNb_{10}O_{35}$ forms at 34:6:60 $Bi_2O_3:Fe_2O_3:Nb_2O_5$ [2] and exhibits hexagonal symmetry ($P6_3/mmc$; $a = 7.432(1)$ Å, $c = 31.881(2)$ Å; $Z = 2$). The second phase, $Bi_{9.3}Fe_{1.1}Nb_{16.9}O_{57.8}$, forms at 34:4:62 $Bi_2O_3:Fe_2O_3:Nb_2O_5$ [2] and is rhombohedral ($R\bar{3}m$; $a = 7.433(1)$ Å, $c = 77.488(2)$ Å; $Z = 3$). The chemical twin planes are $(111)_{py}$ oxygen planes, and the twinning operation produces pairs of corner-connected hexagonal tungsten bronze

(HTB) layers, so the structures may alternatively be described as pyrochlore:HTB unit-cell intergrowth structures [1]. In the hexagonal phase the pyrochlore blocks are doubled with a width of 12 Å, whereas the rhombohedral phase is built from single- and double-pyrochlore blocks with widths 6 and 12 Å, alternating with single-HTB blocks approximately 4 Å in width.

In the Bi_2O_3–Fe_2O_3–Nb_2O_5 phase equilibrium study [2], the compositions of these two ternary phases were found to lie approximately along a straight line joining the end of a cubic pyrochlore phase field to the binary phase reported in earlier work [3] as $4Bi_2O_3:9Nb_2O_5$ ("4:9"). These phase relations are illustrated in Fig. 1. Comparison of the X-ray powder diffraction pattern of the 4:9 phase with those of the two ternary phases revealed systematic similarities, suggesting a close structural relationship among the three

*Corresponding author. Fax: +61 3 9562 8919.
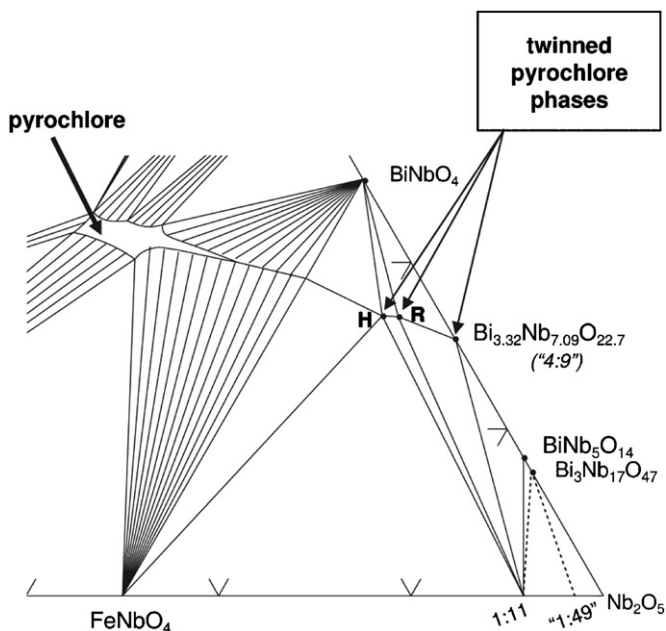E-mail address: ian.grey@csiro.au (I.E. Grey).

Fig. 1. Partial phase diagram for the Bi_2O_3–Fe_2O_3–Nb_2O_5 system (air, 875–1075 °C, Ref. [2]) emphasizing the region containing the four pyrochlore-related phases illustrated in Fig. 5. The pyrochlore solid-solution field and the chemically twinned pyrochlore phases form along a composition line connecting pyrochlore and the end-member $Bi_{3.32}Nb_{7.09}O_{22.7}$ ("4:9"); H = hexagonal $Bi_{5.67}FeNb_{10}O_{35}$, R = rhombohedral $Bi_{9.3}Fe_{1.1}Nb_{16.9}O_{57.8}$.

compounds and pyrochlore. The XRPD pattern for the binary phase can be fully indexed with a hexagonal cell having the same a parameter as the two ternary phases (7.44 Å), and with $c = 19.78$ Å. The periodicity along c was consistent with a chemically twinned pyrochlore model having 6 Å wide pyrochlore blocks, thus suggesting the formation of a systematic structural series with the two ternary phases [1].

The twinned pyrochlore model for the binary phase near 4:9 Bi_2O_3–Nb_2O_5 was confirmed by constructing a model in space group $P6_3/mmc$ and generating the XRPD pattern, which closely matched the observed pattern [1]. However the powder data were inadequate for determining the detailed structural features that occur in the ternary phases such as the small displacements of the Bi atoms from the ideal pyrochlore A-site positions [1]. Single-crystal data are required for elucidating such details; however, the previous phase equilibrium study of the binary Bi_2O_3–Nb_2O_5 system [3] found that the 4:9 phase is stable only in a narrow temperature range (1070–1180 °C) and melts incongruently with an extremely small primary phase field, making the growth of single crystals difficult. Since completing the study on the two ternary phases, we have succeeded in growing small single crystals of the binary phase by prolonged sintering just below the melting point. We report here the results of structural refinements using neutron powder diffraction and single-crystal XRD data.

Recently published dielectric measurements [2] on $Bi_{1.657}Fe_{1.092}Nb_{1.150}O_7$, a member of the parent pyrochlore solid-solution phase, indicated a high relative permittivity

(125 at 200 K, 1 MHz) and a broad low-temperature dielectric relaxation. The dielectric behaviour is similar to that reported for other pyrochlore systems, $A_2B_2O_6O'$, in which there are large, non-correlated static displacements in the A_2O' anti-cristobalite-type sub-network [4–8]. The low-frequency O'–A–O' bending phonon mode has been identified as the major contributor to the ionic dielectric permittivity in cubic bismuth zinc niobate pyrochlores [9,10]. The origin of the dielectric relaxation has been ascribed to the orientational polarizability of the A–O' dipoles created by the static displacements [9–11]. The A_2O' sublattice therefore seems to be the dominant contributor to the dielectric properties of such Bi-containing cubic pyrochlore phases.

The A_2O' sublattices in the Bi–Fe–Nb–O chemically twinned pyrochlore phases exhibit important crystal–chemical differences when compared to the parent pyrochlore phase: the occupancy factors for the A-sites are lower; i.e. $\approx 2/3$ in the chemically twinned phases, and there is no evidence for long-range order between the A atoms (Bi) and the vacancies. In addition, the A-type cations at the interface between the pyrochlore and HTB blocks are coordinated to a single O' anion, rather than to two as in pyrochlore. A study of the dielectric properties of the chemically twinned pyrochlore phases may therefore provide new insights on the influence of the A_2O' sublattice. The dielectric properties of the two ternary phases and the binary 4:9 phase were characterized as a function of temperature and applied frequency and the results are reported here.

2. Experimental methods

2.1. Synthesis and crystal growth of the "4:9" phase

The 4:9 Bi_2O_3:Nb_2O_5 phase ($Bi_8Nb_{18}O_{57}$, PDF 16-0325) was first reported in the extensive study of this binary system by Roth and Waring [3]. The phase was reported to be stable in the temperature range 1070–1180 °C; below 1070 °C a two-phase region of the neighbouring phases ($BiNbO_4$ and $BiNb_5O_{14}$) was stable, and just above 1180 °C the 4:9 phase melted incongruently to liquid and $Bi_3Nb_{17}O_{47}$ (referred to in [3] as "1:6"). The primary phase field indicated for the 4:9 phase was extremely small, less than 5 mol% in width and with perhaps 10 °C of liquid range, and occurred on the Bi-rich side of the 4:9 composition (= 30.77:69.23 Bi_2O_3:Nb_2O_5). Initial crystal-growth experiments were carried out in an attempt to slow-cool a liquid-containing specimen through this small primary 4:9 phase field, i.e. at 32:68 and 33.5:66.5 Bi_2O_3:Nb_2O_5. During the subsolidus pre-reaction of these two compositions at 1150 °C, we observed that no other phases were detectable in the 32:68 specimen by routine X-ray powder diffraction. Careful inspection of the stoichiometric 4:9 specimen, also quenched from 1150 °C, revealed $Bi_3Nb_{17}O_{47}$ as a minor second phase, consistent with the actual stoichiometry of the 4:9 phase occurring at

a slightly higher Bi_2O_3 concentration than 30.77 mol%. As expected, the 33.5:66.5 Bi_2O_3:Nb_2O_5 specimen consisted of the 4:9 phase and a small amount of $BiNbO_4$.

The 4:9 phase was readily prepared in polycrystalline form (12-g batch for powder neutron diffraction) in air by solid-state reaction of Bi_2O_3 (99.999%) and Nb_2O_5 (99.9985%) in the molar ratio 32.00:68.00, respectively. Prior to each heating, the sample was mixed by grinding with an agate mortar and pestle for 15 min and then pelletised. The first heating was carried out on Pt foil at 800° (below the melting point of Bi_2O_3) for 85 h. Subsequent heatings were carried out with the pellets suspended in a Pt bucket in a vertical quench furnace, allowing the specimen to be quickly pulled and plunged into liquid nitrogen. The second heating was carried out at 1130 °C for 40 h, and equilibrated, nearly single-phase material was obtained after a third heating at 1150° for 92 h. A trace amount of $BiNbO_4$ could be observed in the powder XRD pattern, collected using long counting times. These results indicate that the true stoichiometry of the 4:9 phase occurs at a Bi-concentration slightly lower than 32.0 mol%. XRD analysis of a carefully equilibrated specimen at 31.7 mol% Bi_2O_3 showed a trace of $Bi_3Nb_{17}O_{47}$, thus limiting the single phase to a composition close to 31.9:68.1 Bi_2O_3:Nb_2O_5.

Numerous crystal-growth experiments were carried out on the Bi-rich side of this phase, using a 33.5:66.5 Bi_2O_3:Nb_2O_5 specimen in an attempt to access the small primary phase field [3]. Invariably, and regardless of cooling rate, all experiments heated above the solidus (e.g. 1200 °C) to produce a detectable amount of liquid phase resulted in mixtures with no observable 4:9 phase— instead, the products were mixtures dominated by a simple cubic phase ($Bi_{1/3}NbO_3$ with $a \sim 3.94$ Å, as also reported in Ref. [3]) and $BiNbO_4$. Small crystals of the 4:9 phase were finally obtained by the grain-growth method with extended annealing just below the solidus temperature. Approximately 0.3 g of the pre-reacted 33.5:66.5 Bi_2O_3:Nb_2O_5 specimen was placed in a Pt capsule which was sealed by welding and then heated at 1165 °C for 1846 h, followed by air-quenching (removal from furnace). The reaction product featured a small amount of larger, grayish crystals near the top of the capsule, followed by a gap and then a large sintered column of small "glistening" crystals, rounded in shape and yellowish in colour, which readily fell apart with mechanical pressure. The powder XRD pattern of a portion of the composite (grey plus yellow crystals) product indicated nearly single-phase "4:9", with a just-detectable amount of $BiNbO_4$.

Both types of crystals were mounted in epoxy blocks for scanning electron microscope and electron microprobe studies, using a JEOL[1] electron probe microanalyser model

---

[1]Certain commercial equipment and software are identified in order to adequately specify the experimental procedure; recommendation or endorsement by the National Institute of Standards and Technology is not therein implied.

JXA 8900R, operated at 15 kV and 50 nA with 90 s counting for both Bi and Nb. $BiNbO_4$ was used as a reference material. The pale yellow crystals commonly had small rounded crystals of $BiNbO_4$ attached to them, whereas the grey crystals were completely free of the $BiNbO_4$ phase, suggesting different growth conditions. About 30 crystals of both types were analysed.

2.2. Diffraction data collections

Routine X-ray powder diffraction data were obtained with a Philips diffractometer equipped with incident Soller slits, a theta-compensating slit and graphite monochromator, and a scintillation detector. Samples were mounted in welled glass slides. Screening patterns were collected at ambient temperatures using Cu$K\alpha$ radiation over the range 3–70° 2θ with a 0.02° 2θ step size and a 2 s count time. For cell refinement, data were collected over the range 3–90° 2θ with a 0.01° 2θ step size and a 3 s count time. Intensity data measured as relative peak heights above background were obtained using the DATASCAN software package, and processed using JADE. Lattice parameters were refined using JADE (2θ values, Cu$K\alpha_1 = 1.540593$ Å) and observed 2θ line positions that had been corrected using SRM 660 (LaB$_6$) [12] as an external calibrant.

Single-crystal intensity data were collected at room temperature using a Bruker APEX II Kappa CCD diffractometer. The data collection and processing conditions are summarised in Table 1. The CCD intensity data sets were processed to produce an absorption-corrected data file. The structure analysis was conducted within the WinGX program system [13], using SHELX-97 [14] for the refinements.

Powder neutron diffraction data were collected using the BT-1 32-detector neutron powder diffractometer at the NIST Center for Neutron Research, NBSR. The specimen ($\sim$12 g) was loaded in a vanadium container of length 50 mm and diameter 12.4 mm. A Cu(311) monochromator with a 90° take-off angle, $\lambda = 1.5402(2)$ Å, and in-pile collimation of 15 min of arc were used. Data were collected at 293 K over the range 3–169° 2θ with a step size of 0.05°. Refinement of the neutron data was carried out using the Rietveld programs SR5 [15]. The results of the refinement were checked by an independent refinement using GSAS [16].

2.3. Refinement using single-crystal X-ray diffraction data

Application of the assignSG routine in WinGX to the single-crystal data for the 4:9 binary phase showed that the extinctions were consistent with the presence of a c glide plane and a 6_3 screw axis. The same merging R factor (0.054) for equivalent reflections was obtained with both hexagonal and trigonal point groups. The highest symmetry hexagonal space group compatible with the extinctions, $P6_3/mmc$, was selected for a starting model. This space group was used in the successful refinement of the

Table 1
Summary of data collection conditions and refinement parameters for $Bi_{3.32}Nb_{7.09}O_{22.7}$

Formula	$Bi_{3.32}Nb_{7.09}O_{22.7}$
Crystal data	
Cell parameters	$a = 7.4363(1)$
	$c = 19.7587(5)$ Å
Z	2
Space group	$P6_3/mmc$ (no. 194)
Data collect	
Temperature (K)	293
λ (Mo$K\alpha$)	0.71073
Crystal size (mm)	$0.05 \times 0.10 \times 0.15$
Collection mode	4ϕ scans$+2\omega$ scans, $\Delta\phi = 0.5°$
	1795 Images
Count time per frame	75 s
$2\theta_{max}$ (deg.)	70
Reflection range	$-12 \leqslant h, k \leqslant 12; -31 \leqslant l \leqslant 31$
Total no. reflections	18,670
Data completeness	97.8% at res. of 0.62 Å
No. unique reflections	831
No. reflections, $F>4\sigma(F)$	759
Absorption correction	$\mu = 34.8$ mm^{-1}
(Empirical—SADABS)	$T_{min}/T_{max} = 0.52$
R_{merg} on F^2	0.054
Refinement	
No. parameters refined	60
R_1, $F>4\sigma$ (F)	0.026
R_1, all data	0.029
$wR_2(F^2)$*, all data	0.055
GOF	1.12

*$w = 1/[\sigma^2(F_o^2) + (0.02P^2 + 2.5P)$, $P = [2F_c^2 + Max(F_o^2, 0)]/3$ from Ref. [14].

Table 2
Atomic coordinates ($\times 10^4$) and equivalent isotropic displacement parameters ($Å^2 \times 10^3$) for $Bi_{3.32}Nb_{7.09}O_{22.7}$. U(eq) is defined as one third of the trace of the orthogonalized U_{ij} tensor

Atom	Site	x	y	z	U(eq)
Nb(1)	2a	0	0	0	13(1)
Nb(2)	12k	1665(1)	3331(1)	1564(1)	13(1)
O(1)	12k	1292(2)	2584(4)	549(1)	14(1)
O(2)	12k	4589(2)	9178(4)	1322(1)	14(1)
O(3)	12k	8733(2)	7465(4)	1668(1)	14(1)
O(4)	6h	2015(2)	4030(5)	2500	12(1)
O(5)[a]	4f	3333	6667	5484(7)	84(5)
Bi(1A)[a]	12i	5455(7)	0	0	20(2)
Bi(1B)[a]	12k	4906(3)	9813(7)	174(5)	20(3)
Bi(2A)[a]	12k	6073(6)	3037(3)	1559(2)	35(1)
Bi(2B)[a]	12k	6356(8)	2712(15)	1612(4)	4(2)

[a] Fractional site occupancies: O(5) 0.88(3), Bi(1A) 0.24(1), Bi(1B) 0.13(2), Bi(2A) 0.156(4), Bi(2B) 0.042(4).

Table 3
Anisotropic displacement parameters ($Å^2 \times 10^3$) for $Bi_{3.32}Nb_{7.09}O_{22.7}$

	U_{11}	U_{12}	U_{33}	U_{23}	U_{13}	U_{12}
Nb(1)	18(1)	18(1)	2(1)	0	0	9(1)
Nb(2)	17(1)	10(1)	9(1)	0(1)	0(1)	5(1)
O(1)	21(1)	13(1)	5(1)	−5(1)	−2(1)	7(1)
O(2)	10(1)	21(1)	15(1)	6(1)	3(1)	11(1)
O(3)	12(1)	22(1)	10(1)	3(1)	1(1)	11(1)
O(4)	18(1)	13(1)	2(1)	0	0	7(1)
O(5)	60(5)	60(5)	131(12)	0	0	30(2)
Bi(1A)	15(1)	20(1)	28(5)	−1(2)	0(1)	10(1)
Bi(1B)	33(6)	21(1)	2(2)	5(1)	3(1)	11(1)
Bi(2A)[a]	13(1)	59(2)	17(1)	−1(1)	−3(1)	6(1)

The anisotropic displacement factor exponent takes the form: $-2p^2[h^2a^{*2}U_{11} + \cdots + 2hka^*b^*U_{12}]$.
[a] Bi(2B) not refined anisotropically because of low fractional occupancy.

hexagonal ternary phase $Bi_{5.67}FeNb_{10}O_{35}$ [1]. Based on the structure of the ternary phase, a model was readily constructed for the binary phase, with 6 Å wide pyrochlore blocks along [001], in place of the 12 Å blocks in the ternary phase.

In the starting model, the Bi atoms were located at the ideal *A* sites in the pyrochlore blocks (i.e. at the centres of the hexagonal rings in the HTB layers). The ideal *A* sites are at (1/2,0,0) and (2/3,1/3,1/6). However this model could not be refined below an R_1 value of 0.3. Difference Fourier maps showed that the Bi atoms were displaced by $\sim$0.3 Å from the ideal *A*-site positions. Introduction of split Bi atom sites and refinement of coordinates, isotropic displacement parameters, and Bi and O′ (O(5)) site occupancies converged at an R_1 value of 0.10. Conversion to anisotropic displacement parameters resulted in final convergence at an $R_1 = 0.029$ for all reflections. Further refinement details are given in Table 1. The coordinates and equivalent isotropic displacement parameters from the refinement are reported in Table 2. The anisotropic displacement parameters are given in Table 3.

2.4. Refinement using powder diffraction data

The atomic coordinates obtained from the single-crystal refinement were used as starting parameters for the refinement of the powder neutron data. The coordinates for the split Bi atom sites were considered to be better determined from the single-crystal data, because of the much stronger relative contribution of Bi using X-ray data and the higher resolution of the data ($d>0.62$ Å, compared with $d>0.77$ Å for the neutron data). These coordinates were thus fixed during the refinement of the powder neutron diffraction data. Refinements were made of the profile parameters, coordinates of the niobium and oxygen atoms, isotropic displacement parameters for all atoms, and site occupancies for O(5) and the Bi sites. The results of the refinement are given in Table 4. A comparison of the observed and calculated powder neutron diffraction patterns is shown in Fig. 2.

The experimental, indexed X-ray powder diffraction pattern for the 4:9 phase is given in Table 5 along with the unit-cell parameters obtained by least-squares refinement of the data. The cell parameters reported in Table 5 differ

Table 4
Results from Rietveld refinement of powder neutron diffraction data for $Bi_{3.32}Nb_{7.09}O_{22.7}$. Atomic coordinates ($\times 10^4$), isotropic displacement parameters ($\mathring{A}^2 \times 10^3$)

Atom	Site	x	y	z	U(iso)
Nb(1)	2a	0	0	0	16(1)
Nb(2)	12k	1668(1)	3331(1)	1566(1)	11.4(2)
O(1)	12k	1287(2)	2574(4)	550(1)	14.8(4)
O(2)	12k	4592(2)	9184(4)	1322(1)	16.8(4)
O(3)	12k	8727(2)	7454(4)	1672(1)	13.4(4)
O(4)	6h	2005(2)	4010(5)	2500	11.1(6)
O(5)[a]	4f	3333	6667	5473(4)	66(3)
Bi(1A)[a]	12i	5455	0	0	22(3)
Bi(1B)[a]	12k	4906	9812	174	26(5)
Bi(2A)[a]	12k	6073	3037	1559	48(5)
Bi(2B)[a]	12k	6356	2712	1612	25(5)

$R_{wp} = 5.8\%$, $R_B = 3.6\%$, GOF = 5.9.

[a] Fractional site occupancies: O(5) 0.85(1), Bi(1A) 0.23(1), Bi(1B) 0.14(1), Bi(2A) 0.14(1), Bi(2B) 0.08(1).
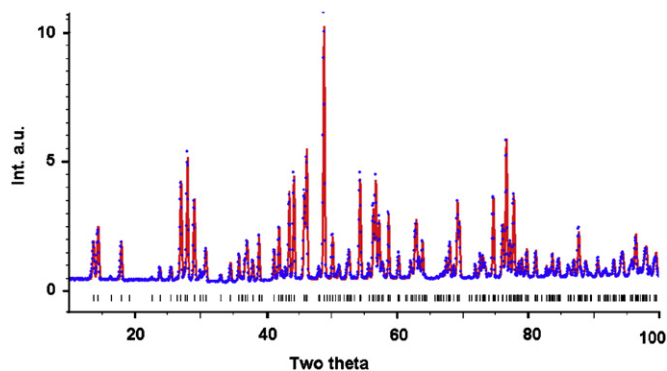

Fig. 2. Calculated (solid line) and experimental (dots) neutron diffraction pattern for $Bi_{3.32}Nb_{7.09}O_{22.7}$, $\lambda = 1.5406\,\mathring{A}$. The positions of the Bragg reflections are shown by the short vertical lines below the pattern.

Table 5
Observed X-ray powder diffraction data for $Bi_{3.32}Nb_{7.09}O_{22.7}$ ($P6_3/mmc$; $a = 7.4481(2)$, $c = 19.779(1)\,\mathring{A}$; $\lambda = 1.540593\,\mathring{A}$)

(hkl)	$2\theta_{obs}$	I_{obs}	$2\theta_{calc}$	$\Delta 2\theta$	d_{obs}
(002)	8.929	11	8.934	0.005	9.896
(004)	17.903	4	17.924	0.020	4.9504
(110)	23.868	1	23.875	0.007	3.7251
(112)	25.537	1	25.538	0.001	3.4853
(006)	27.014	100	27.026	0.012	3.2980
(201)	28.001	83	28.009	0.008	3.1839
(202)	29.088	96	29.100	0.012	3.0674
(203)	30.836	7	30.839	0.004	2.8974
(204)	33.127	91	33.136	0.009	2.7021
(107)	34.623	2	34.629	0.007	2.5887
(205)	35.889	44	35.897	0.008	2.5002
(008)	36.293	11	36.306	0.013	2.4733
(210)	36.834	2	36.838	0.003	2.4382
(211)	37.125	1	37.126	0.001	2.4197
(212)	37.970	2	37.982	0.012	2.3678
(108)	39.000	5	38.982	−0.018	2.3076
(300)	42.001	1	41.987	−0.014	2.1494
(207)	42.498	17	42.500	0.002	2.1254
(215)	43.567	2	43.572	0.006	2.0757

Table 5 (continued)

(hkl)	$2\theta_{obs}$	I_{obs}	$2\theta_{calc}$	$\Delta 2\theta$	d_{obs}
(118)	43.910	1	43.921	0.011	2.0603
(303)	44.269	3	44.275	0.006	2.0444
(0010)	45.828	8	45.840	0.012	1.9784
(304)	45.997	6	45.992	−0.005	1.9715
(208)	46.228	35	46.229	0.002	1.9622
(220)	48.872	60	48.874	0.001	1.8621
(222)	49.776	2	49.790	0.014	1.8304
(209)	50.184	15	50.193	0.009	1.8164
(310)	51.001	2	51.009	0.008	1.7892
(311)	51.227	1	51.232	0.005	1.7819
(312)	51.895	<1	51.898	0.003	1.7605
(2010)	54.366	48	54.368	0.002	1.6862
(0012)	55.728	19	55.723	−0.006	1.6481
(315)	56.417	2	56.402	−0.015	1.6296
(226)	56.735	47	56.734	−0.001	1.6212
(400)	57.079	2	57.069	−0.010	1.6123
(401)	57.284	16	57.276	−0.008	1.6070
(402)	57.898	12	57.893	−0.005	1.5914
(2011)	58.742	30	58.743	0.001	1.5706
(404)	60.325	19	60.324	−0.001	1.5331
(405)	62.105	12	62.109	0.004	1.4933
(228)	62.366	7	62.381	0.015	1.4877
(320)	62.730	2	62.738	0.008	1.4799
(321)	62.933	2	62.933	0.000	1.4757
(3010)	63.910	1	63.899	−0.011	1.4554
(0014)	66.071	5	66.080	0.008	1.4130
(411)	66.555	1	66.548	−0.007	1.4039
(407)	66.737	3	66.734	−0.003	1.4005
(325)	67.532	1	67.528	−0.004	1.3859
(2013)	68.079	<1	68.082	0.004	1.3761
(2210)	69.251	4	69.244	−0.007	1.3557
(408)	69.546	7	69.543	−0.003	1.3506
(409)	72.662	3	72.667	0.005	1.3002
(416)	73.041	4	73.033	−0.007	1.2944
(501)	73.502	<1	73.508	0.005	1.2874
(4010)	76.100	11	76.096	−0.004	1.2498
(3013)	76.655	<1	76.664	0.009	1.2421
(0016)	77.087	2	77.087	0.001	1.2362
(2212)	77.240	17	77.237	−0.004	1.2341
(329)	77.742	1	77.739	−0.003	1.2274
(2015)	78.271	7	78.264	−0.007	1.2205
(421)	78.549	8	78.561	0.012	1.2168
(422)	79.093	7	79.093	−0.001	1.2098
(4011)	79.830	7	79.828	−0.002	1.2005
(424)	81.214	9	81.210	−0.004	1.1835
(425)	82.789	7	82.789	0.000	1.1649
(510)	83.350	1	83.351	0.001	1.1585
(2016)	83.718	11	83.721	0.002	1.1543
(508)	84.680	1	84.676	−0.004	1.1437
(2214)	86.375	5	86.377	0.002	1.1255
(427)	86.974	3	86.978	0.004	1.1193
(515)	87.712	2	87.710	−0.001	1.1118
(4013)	88.229	<1	88.224	−0.005	1.1066
(3212)	88.784	1	88.782	−0.002	1.1011
(0018)	89.013	2	89.014	0.002	1.0989
(2017)	89.476	7	89.468	−0.007	1.0944

significantly from those determined from the single-crystal data collection, see Table 1. The former should be considered the more accurate, see Section 2.2 for refinement conditions.

2.5. Characterisation of dielectric properties

Dielectric properties were measured using disks (≈ 6 mm in diameter, 0.7 mm thick) pressed from pre-equilibrated powders and sintered at 1100 °C (ternary phases) or 1150 °C (4:9 phase) for 4 h. The molar compositions of the specimens were $Bi_2O_3:Fe_2O_3:Nb_2O_5 = 34:6:60$ and 34:4:62 for the hexagonal and rhombohedral ternary phases, respectively, and 32:68 $Bi_2O_3:Nb_2O_5$ for the 4:9 phase. Densities were determined geometrically. Specimens were then polished to obtain planar surfaces and gold electrodes (75 nm thick) were sputtered onto the pellet surfaces to form parallel plate capacitors. The capacitance and dielectric loss were measured using an Agilent 4284 LCR metre at frequencies varying from 1 kHz to 1 MHz. Reported permittivity data have been corrected to theoretical density. The sample temperature was varied between 110 and 475 K using a programmable 9023 Delta Design controller. Typical uncertainties in the permittivity data are on the order of 5% and are dominated by the geometric estimates of porosity.

3. Results and discussion

3.1. Composition of the binary "4:9" phase

The average electron microprobe results are 44.5 wt% Bi_2O_3, 54.6 wt% Nb_2O_5 for the pale yellow crystals and 44.4 wt Bi_2O_3, 55.1 wt% Nb_2O_5 for the grey crystals. These differences are likely insignificant as the analytical errors due solely to counting statistics are of the order of 0.3 wt% for Bi_2O_3 and 0.2 wt% for Nb_2O_5.

The ideal (all sites fully occupied) asymmetric-unit formula for chemically twinned pyrochlore with 6 Å wide pyrochlore blocks is $A_5B_7O_{21}O'_2$ [1]. However the A sites are partially occupied, and this entails partial occupancy of the O' sites as the O' atoms bond only to the A atoms. The occupancy factors for the O' site (O(5)) obtained from the single crystal and powder neutron refinements agree to within one e.s.d., giving 1.70(2) O' per asymmetric unit. Adding the fully occupied O sites gives 22.7 oxygen atoms per formula unit. Scaling the electron microprobe analyses for Nb and Bi to 22.7 oxygen atoms then gives a formula of $Bi_{3.3}Nb_{7.1}O_{22.7}$.

Written in structural form, in terms of A and B sites, the formula is $[Bi_{3.3}Nb_{0.1}\Upsilon_{1.6}]Nb_7O_{22.7}$, $\Upsilon =$ vacancy, which requires that 2% of the A sites contain Nb. The presence of vacancies at the A sites precludes a sensible refinement of Bi/Nb in these sites. However, in refinements with Bi atoms only at the A sites, the sum of the refined occupancies per asymmetric unit is 3.4(2) Bi from the single-crystal refinement and 3.5(2) from the powder neutron refinement. The two results agree with each other and with the formula from the microprobe analyses within 1 e.s.d.. The microprobe analyses give 31.7 mol% Bi_2O_3, which compares with 31.9 mol% from the current phase equilibria studies and 30.8 mol% for the originally proposed 4:9 molar ratio [3].

Given the errors associated with the probe analysis, the results are consistent with those from the phase equilibria studies, and the most likely composition of the 4:9 phase is 31.9:68.1 $Bi_2O_3:Nb_2O_5$ (or $Bi_{3.32}Nb_{7.09}O_{22.7}$).

3.2. Description of the structure of $Bi_{3.32}Nb_{7.09}O_{22.7}$

A polyhedral representation of the structure of $Bi_{3.32}Nb_{7.09}O_{22.7}$ is shown in projection along [110] in Fig. 3. The corner-connected octahedral framework has the same composition, B_2O_6, as the frameworks in both the pyrochlore and HTB structures. As seen from Fig. 3, the structure may be described as a 1:1 intergrowth of these two structure types along (001) (equivalent to $\{111\}_{py}$ for cubic pyrochlore). The blocks of pyrochlore, 6.2 Å thick and HTB, 3.7 Å thick, represent the smallest repeating units of each structure. Formally, the intergrowth structure can be derived from the pyrochlore structure by periodic unit-cell scale twinning at $\{111\}_{py}$ planes of oxygen atoms, O(4) in Fig. 3. The term "chemical twinning" has been proposed for this type of operation [17]. The twin planes, shown by the thick arrows in Fig. 3, are separated by $0.5c = 9.88$ Å.

The pyrochlore A atom sites are partially occupied by Bi. From the single-crystal refinement, the fractional occupation is 0.74(6) for the Bi(1) site centred at (1/2,0,0) and 0.59(2) for the Bi(2) site centred at (2/3,1/3,1/6), giving an
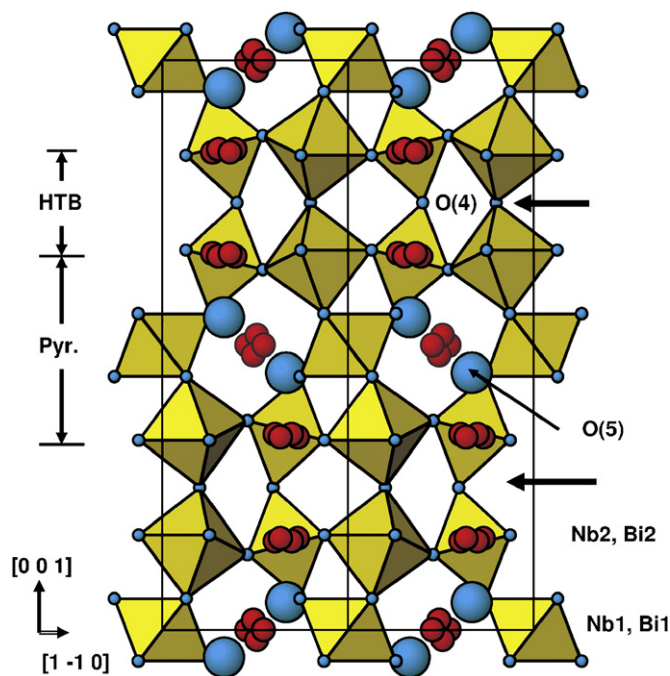

Fig. 3. Polyhedral representation of the structure of $Bi_{3.32}Nb_{7.09}O_{22.7}$, viewed along [110]. The red spheres denote Bi atoms and the larger blue spheres correspond to O(5). The structure is built from slabs of the pyrochlore-type (Py) and hexagonal-tungsten–bronze-type (HTB) structures which alternate along (001), as shown. Alternatively, the structure is derived by chemical twinning of pyrochlore at $\{111\}_{py}$ planes of oxygen atoms (O(4), shown by the thick arrows).

average occupancy of 0.67. In both sites the Bi atoms are displaced from the ideal positions. The Bi(1) site, in the pyrochlore block, splits into two pairs; Bi(1A) and Bi(1B), displaced by 0.34 and 0.36 Å from (1/2,0,0). The Bi(2) site, located in the HTB block, splits into two triangular groups, Bi(2A) and Bi(2B), displaced by 0.33 and 0.34 Å, respectively, from the ideal site. The six Bi(2) sites form an almost planar hexagonal cluster in the (001) plane. The six split Bi(2) atoms are displaced along equivalent $\langle 1\bar{1}0 \rangle$ directions, towards the six oxygen atoms that form the hexagonal rings in the HTB layers, (O(2) and O(3) in Table 2). This disposition of split Bi sites in the HTB layers is the same as found for the two ternary chemically twinned pyrochlore compounds [1]. Another feature in common with the ternary phases is the lower fractional occupancy of the Bi sites in the HTB layers compared with the pyrochlore block sites [1].

The coordination environments for Bi(1) and Bi(2) differ significantly: the Bi(2) atoms are bonded to only one O′ anion (O(5)) whereas the Bi(1) atoms are symmetrically bonded to two O′ anions as in the parent pyrochlore structure. The coordination environments for Bi(1) and Bi(2) are illustrated for comparison in Fig. 4. As seen from Table 6, the singly coordinated distances of Bi(2A) and Bi(2B) to O(5), 2.16(1) and 2.26(1) Å, respectively, are considerably shorter than the 2-coordinated distances of Bi(1A) and Bi(1B) to O(5), 2.37 (× 2) and 2.35, 2.41 Å, respectively. By analogy with Bi-containing pyrochlores [2,7], displacements of the O′ atoms from the ideal pyrochlore position are expected, and should reflect which of the Bi sites are occupied or vacant. Although we were unable to resolve such displacements for O(5), its anisotropic displacement parameters are very large (Table 3) and correspond to an elongation of the ellipsoid along [001].

The structures of pyrochlore and the three chemically twinned derivative phases are illustrated in Fig. 5 for comparison. The Bi–Fe–Nb–O pyrochlore (Fig. 5a) and $Bi_{3.32}Nb_{7.09}O_{22.7}$ (Fig. 5d) are the end-members of the series. As shown, the structure of hexagonal $Bi_{5.67}FeNb_{10}O_{35}$ (Fig. 5b) (34:6:60 Bi_2O_3:Fe_2O_3:Nb_2O_5) [1] is built from

Table 6
Selected bond lengths in $Bi_{3.32}Nb_{7.09}O_{22.7}$

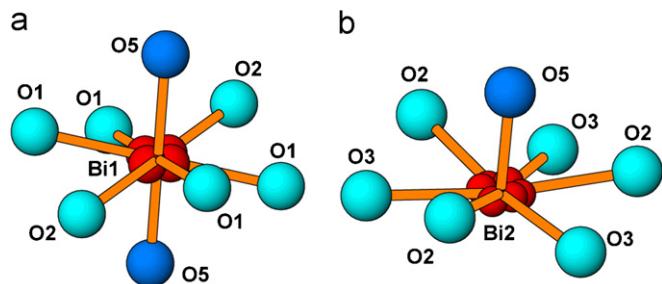| M–O	Distance
Nb(1)–O(1) × 6	1.987(2)
Nb(2)–O(4)	1.903(1)
Nb(2)–O(3) × 2	1.951(1)
Nb(2)–O(2) × 2	1.996(1)
Nb(2)–O(1)	2.062(2)
Bi(1A)–O(1) × 2	2.373(5)
Bi(1A)–O(5) × 2	2.374(6)
Bi(1A)–O(2) × 2	2.686(3)
Bi(1B)–O(2)	2.31(1)
Bi(1B)–O(5)	2.349(4)
Bi(1B)–O(5)	2.406(8)
Bi(1B)–O(1) × 2	2.498(5)
Bi(2A)–O(5)	2.16(1)
Bi(2A)–O(3)	2.289(5)
Bi(2A)–O(2) × 2	2.550(4)
Bi(2B)–O(5)	2.26(1)
Bi(2B)–O(2)	2.35(1)
Bi(2B)–O(3) × 2	2.487(5)

Fig. 4. Comparison of coordination for (a) Bi(1) and (b) Bi(2) in $Bi_{3.32}Nb_{7.09}O_{22.7}$. In (a), the two Bi(1A) sites displace towards O(1)–O(1) edges whereas each Bi(1B) site displaces towards an O(2). In (b), the three Bi(2A) sites displace towards O(3), whereas the three Bi(2B) sites displace towards O(2), forming an almost planar hexagonal cluster. The Bi–O distances are given in Table 6.
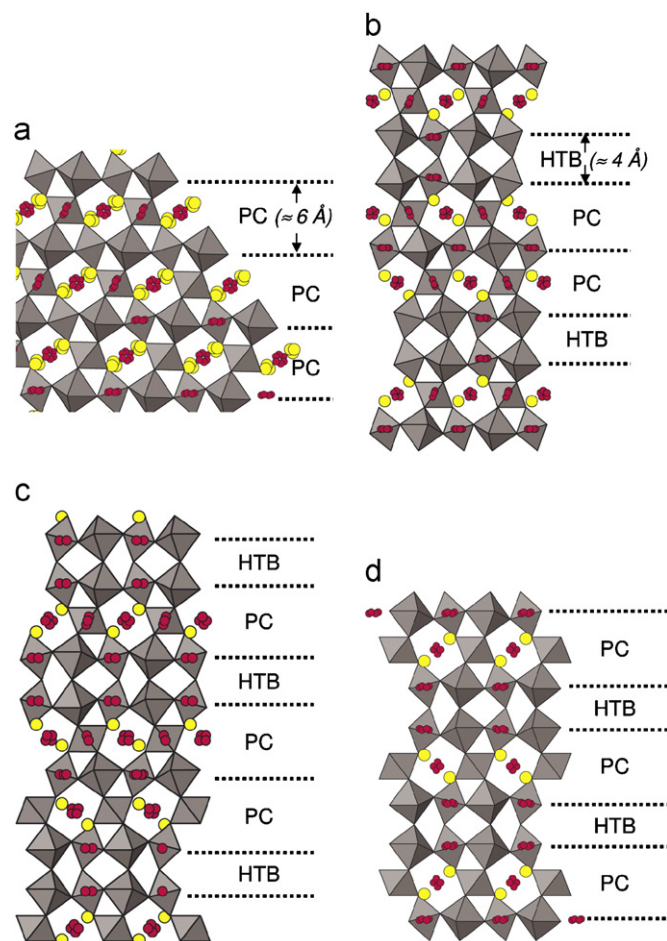
Fig. 5. Structures of the four pyrochlore-related phases (labelled by Bi_2O_3:Fe_2O_3:Nb_2O_5 composition) shown in Fig. 1, PC = pyrochlore block, HTB = hexagonal tungsten bronze: (a) the parent pyrochlore, $Bi_{1.657}Fe_{1.092}Nb_{1.150}O_7$ (44:27:29) [2], (b) hexagonal $Bi_{5.67}FeNb_{10}O_{35}$ (34:6:60) [1], (c) rhombohedral $Bi_{9.3}Fe_{1.1}Nb_{16.9}O_{57.8}$ (34:4:62) [1], and (d) the binary $Bi_{3.32}Nb_{7.09}O_{22.7}$ phase (31.9:0:68.1).

alternating double blocks of pyrochlore and HTB, whereas that of rhombohedral $Bi_{9.3}Fe_{1.1}Nb_{16.9}O_{57.8}$ (Fig. 5c) (34:4:62 Bi_2O_3:Fe_2O_3:Nb_2O_5) [1], features HTB blocks that alternate with single- and double-pyrochlore

blocks. The structure of the end-member binary "4:9" phase $Bi_{3.32}Nb_{7.09}O_{22.7}$ (Fig. 5d) (31.9:68.1 Bi_2O_3:Nb_2O_5) exhibits a simpler pattern of alternating single blocks of pyrochlore and HTB.

3.3. Dielectric properties

The dielectric properties as a function of temperature and frequency for $Bi_{3.32}Nb_{7.09}O_{22.7}$ and the two related ternary phases, $Bi_{9.3}Fe_{1.1}Nb_{16.9}O_{57.8}$ and $Bi_{5.67}FeNb_{10}O_{35}$, are shown in Figs. 6a–c, respectively. As observed for the parent Bi–Fe–Nb–O pyrochlore [2], all of these pyrochlore derivatives exhibit broad, low-temperature dielectric relaxation characteristic of bismuth-based pyrochlores [10,18,19]; that is, with increasing measuring frequency the peak of the dielectric loss shifts towards higher temperatures and the width and maximum of the dielectric loss peak increases. The upturns in dielectric loss at higher temperatures indicate that the samples become conductive. Compared to the parent pyrochlore phase [2], the chemically twinned derivatives exhibit higher relative permittivities, and somewhat lower temperatures at which the peaks of the dielectric losses occur.

To better understand the origin of these differences, it is important to note that the major crystal-chemical difference between pyrochlore and the twinned pyrochlore structures is the highly asymmetric coordination environment of the Bi(2) atoms, located in the HTB blocks, which are bonded to O(5) on only one side of the hexagonal rings (instead of two in pyrochlore). This arrangement results in a highly polarisable environment and therefore, higher dielectric permittivities are expected for the chemically twinned pyrochlores. Along the series of phases, the fraction of Bi content located in the HTB blocks increases, from zero in the pyrochlore end-member $Bi_{1.657}Fe_{1.092}Nb_{1.150}O_7$ (Fig. 5a), to 0.23 for

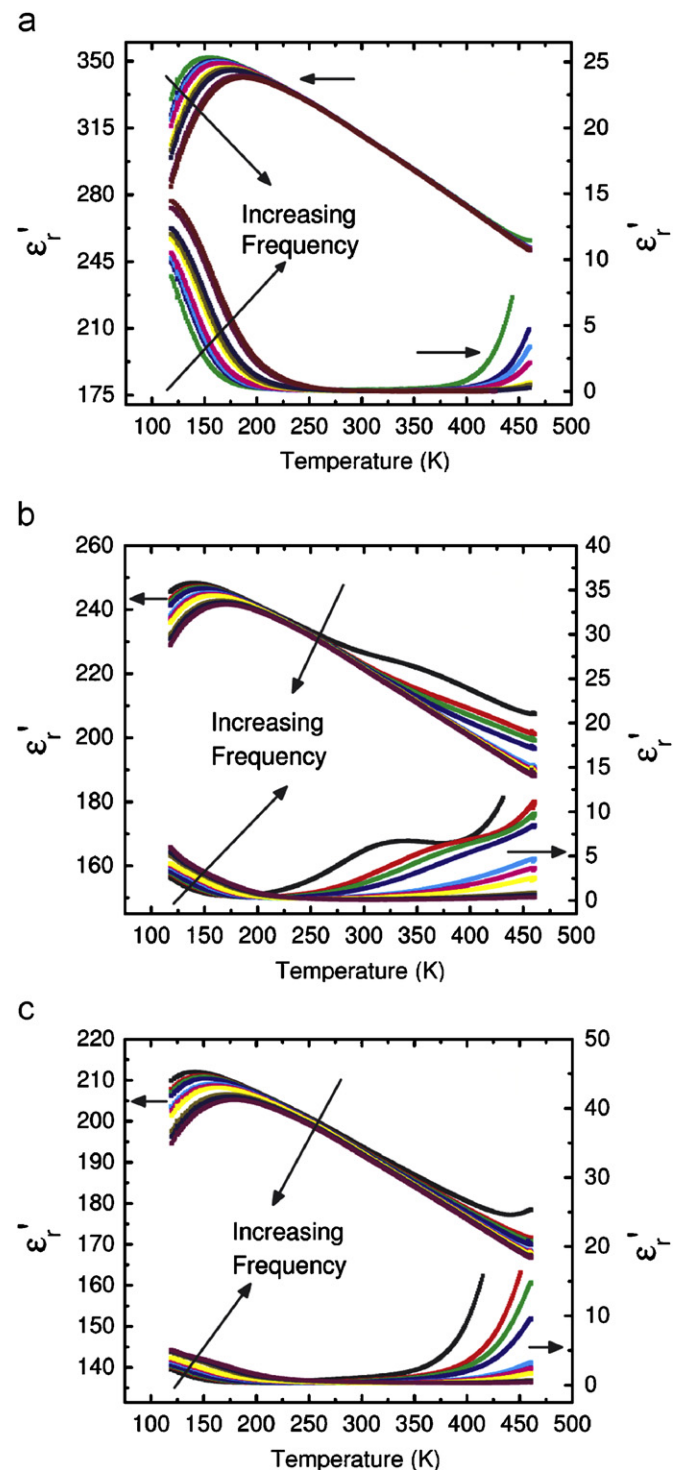Fig. 6. Relative dielectric permittivity (ε_r'; corrected for porosity) and dielectric loss factor (ε_r'') for (a) $Bi_{3.32}Nb_{7.09}O_{22.7}$, (b) rhombohedral $Bi_{9.3}Fe_{1.1}Nb_{16.9}O_{57.8}$, and (c) hexagonal $Bi_{5.67}FeNb_{10}O_{35}$. In all cases, the measuring frequencies are 1, 4, 6, 8, 10, 40, 60, 80, 100, 400, 600, 800 and 1000 kHz.
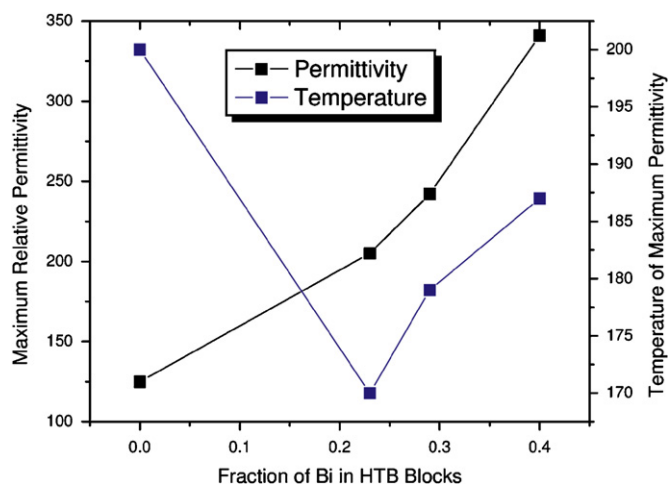

Fig. 7. Maximum relative permittivity at 1 MHz (left) and temperature at which the maximum occurs (right) vs. fraction of Bi in the HTB blocks for the four structurally related phases (Figs. 5a–d).

$Bi_{5.67}FeNb_{10}O_{35}$ (Fig. 5b), to 0.29 for $Bi_{9.3}Fe_{1.1}Nb_{16.9}O_{57.8}$ (Fig. 5c), and to 0.40 for the binary $Bi_{3.32}Nb_{7.09}O_{22.7}$ phase (Fig. 5d). The relative permittivity (1 MHz, ~175 K) for the four compounds increases smoothly with increasing fraction of Bi in the HTB block as illustrated in Fig. 7. The temperature at which the dielectric permittivity maximum occurs in the four related phases is also plotted in Fig. 7. Interestingly, the inclusion of Bi in the HTB blocks lowers the temperature for the maximum compared to pyrochlore; however, the temperature then increases as the fraction becomes larger. Similar behaviour has been observed for zinc and magnesium bismuth niobate pyrochlores when the Bi content was modified [6]. Although the reasons for this behaviour are unclear at this time, this observed trend may prove useful for understanding the peculiar dielectric relaxation of pyrochlore dielectrics.

4. Conclusions

The crystal structure of the phase reported in early studies to occur at 4:9 Bi_2O_3:Nb_2O_5 has been determined using single-crystal X-ray and powder neutron diffraction. The present study indicated that the actual composition of the 4:9 phase is $Bi_{3.32}Nb_{7.09}O_{22.7}$. This binary compound is the end-member of a family of four phases which form along a line between it and the pyrochlore phase field in the Bi_2O_3:Fe_2O_3:Nb_2O_5 system. The structures are derived from pyrochlore by chemical twinning, and can also be described as unit-cell intergrowths of the pyrochlore and hexagonal tungsten bronze (HTB) structures. The dielectric properties of the three chemically twinned pyrochlore phases, $Bi_{3.32}Nb_{7.09}O_{22.7}$, $Bi_{9.3}Fe_{1.1}Nb_{16.9}O_{57.8}$ and $Bi_{5.67}FeNb_{10}O_{35}$, were characterized. All exhibit low-temperature, broad dielectric relaxation similar to that of the parent Bi–Fe–Nb–O pyrochlore end-member. The chemically twinned pyrochlore derivatives exhibit higher relative permittivities than pyrochlore, which was attributed to the highly asymmetric coordination environment of Bi located within the HTB portions of the structures; the magnitude of the relative permittivity increases with the proportion of Bi occupying the HTB blocks.

References

[1] I.E. Grey, W.G. Mumme, T.A. Vanderah, R.S. Roth, C. Bougerol, J. Solid State Chem. 180 (2007) 158–166.
[2] M.W. Lufaso, T.A. Vanderah, I.M. Pazos, I. Levin, R.S. Roth, J.C. Nino, V. Provenzano, P.K. Schenck, J. Solid State Chem. 179 (2006) 3900–3910.
[3] R.S. Roth, J.L. Waring, J. Res. NBS 66A (6) (1962) 451–463;
R.S. Roth, J.L. Waring, Phase Equilibria Diagrams, vol. I, The American Ceramic Society, Westerville, OH. Fig. 324.
[4] M. Valant, P.K. Davies, J. Mater. Sci. 34 (1999) 5437–5442.
[5] T.A. Vanderah, I. Levin, M.W. Lufaso, Eur. J. Inorg. Chem. 14 (2005) 2895–2901.
[6] J.C. Nino, H.J. Youn, M.T. Lanagan, C.A. Randall, J. Mater. Res. 17 (2002) 1178–1182.
[7] B. Melot, E. Rodriguez, Th. Proffen, M.A. Hayward, R. Seshadri, Mat. Res. Bull. 41 (2006) 961–966.
[8] S.S. Kim, W.J. Kim, J. Crystal Growth 281 (2005) 432–439.
[9] S. Kamba, V. Porokhonskyy, A. Pashkin, V. Bovtun, J. Petzelt, J.C. Nino, S. Trolier-McKinstry, M.T. Lanagan, C.A. Randall, Phys. Rev. B 66 (2002) 05416 (1–8).
[10] J.C. Nino, M.T. Lanagan, C.A. Randall, S. Kamba, Appl. Phys. Lett. 81 (2002) 4404–4406.
[11] N.N. Kolpakova, R. Margraf, M. Polomska, J. Phys.: Condens. Matter 6 (1994) 2787–2798.
[12] C.R. Hubbard, Y. Zhang, R.L. McKenzie, Certificate of Analysis, SRM 660, National Institute of Standards and Technology, Gaithersburg, MD, 1989, p. 20899.
[13] L.J. Farrugia, J. Appl. Crystallogr. 32 (1999) 837–838.
[14] G.M. Sheldrick, SHELXL, University of Gottingen, Germany, 1997.
[15] R.J. Hill, C.J. Howard, A computer program for Rietveld analysis of fixed wavelength X-ray and neutron powder diffraction patterns, in: AAEC Report Number M112. Australian Atomic Energy Commission, Sydney, Australia, 1986.
[16] A.C. Larsen, R.B. Von Dreele. General Structure Analysis System (GSAS), Los Alamos National Laboratory report LAUR86-748, 1994.
[17] S. Andersson, B.G. Hyde, J. Solid State Chem. 9 (1974) 92–101.
[18] J.C. Nino, M.T. Lanagan, C.A. Randall, J. Appl. Phys. 89 (2001) 4512–4516.
[19] S. Kamba, V. Porokhonskyy, A. Pashkin, V. Bovtun, J. Petzelt, J.C. Nino, S. Trolier-McKinstry, M.T. Lanagan, C.A. Randall, Phys. Rev. B 66 (2002) 54106.